Supplementary Materials for "Probing a dissipative phase transition with a trapped ion through reservoir engineering"

M.-L. Cai*[1], Z.-D. Liu*[1], Y. Jiang*[1], Y.-K. Wu[1], Q.-X. Mei[1], W.-D. Zhao[1], L. He[1], X. Zhang[2,1], Z.-C. Zhou[1,3], L.-M. Duan†[1]

[1] *Center for Quantum Information, Institute for Interdisciplinary Information Sciences, Tsinghua University, Beijing 100084, PR China*

[2] *Department of Physics, Renmin University, Beijing 100084, PR China and*

[3] *Beijing Academy of Quantum Information Sciences, Beijing 100193, PR China*

EXPERIMENTAL SETUP

Our experimental setup is a single $^{171}\mathrm{Yb}^{+}$ ion in a linear Paul trap. The spin state is encoded in the $|\downarrow\rangle = \left|^2S_{1/2}, F=0, m_F=0\right\rangle$ and the $|\uparrow\rangle = \left|^2S_{1/2}, F=1, m_F=0\right\rangle$ levels of the ion with atomic transition frequency $\omega_0 = 2\pi \times 12.6428\,\mathrm{GHz}$, and the bosonic mode is encoded in a radial oscillation mode with secular frequency $\omega_\mathrm{m} = 2\pi \times 2.35\,\mathrm{MHz}$.

We use counter-propagating 355 nm pulsed laser beams with a repetition rate $\omega_\mathrm{rep} \approx 2\pi \times 118.415\,\mathrm{MHz}$ and a bandwidth of about 200 GHz to manipulate the qubit through Raman transition. Two acousto-optic modulators (AOMs) are used to fine-tune the frequency and the amplitude of the Raman transitions. More details can be found in Ref. [24] of the main text.

MEASUREMENT OF PHONON POPULATION

We follow the standard method of Ref. [15,24] of the main text to fit the phonon state population. Note that after each cycle of coherent drive and dissipation, the spin state is already pumped to $|\downarrow\rangle$, so we only need to apply a blue sideband pulse with various duration t and measure the spin-up state population $P_\uparrow$ afterwards. It can be fitted by

$$P_\uparrow(t) = \frac{1}{2}\left[1 - \sum_{k=0}^{k_\mathrm{max}} p_k e^{-\gamma_k t}\cos(\Omega_{k,k+1}t)\right], \tag{S1}$$

where p_k is the occupation in the Fock state $|k\rangle$, γ_k a number-state-dependent empirical decay rate of the Rabi oscillation, $\Omega_{k,k+1} \propto \sqrt{k+1}$ the number-state-dependent sideband Rabi frequency, and k_max the cutoff in the phonon number. After fitting the phonon state population $P = (p_0, p_1, \cdots)^T$ with its covariance matrix Σ, we can compute the average phonon number $\bar{n} = N \cdot P$ where $N = (0, 1, \cdots)$ is a row vector representing the phonon number basis. Assuming the fitted parameters follow a joint Gaussian distribution, we can estimate the variance of $\bar{n}$ as $\sigma_{\bar{n}}^2 = N\Sigma N^T$, hence the error bar of the average phonon number of one standard deviation is $\sigma_{\bar{n}} = \sqrt{N\Sigma N^T}$.

THE CALIBRATION OF MODEL PARAMETERS

In the quantum Rabi model Hamiltonian (see formula (1) in the main text), three parameters ω_a, ω_f and λ fully determine the Hamiltonian. In experiment simulation with trapped ion, $\omega_a = (\delta_b + \delta_r)/2$, $\omega_f = (\delta_b - \delta_r)/2$ and $\lambda = \Omega_\mathrm{SB}/2$ where $\delta_{b\,(r)}$ is the detuning of the differential Raman laser frequency from the blue (red) sideband of the motional mode and Ω_SB is the sideband Rabi frequency. Before every experiment, we need to calibrate the actual value of δ_b, δ_r and Ω_SB. In terms of the calibration of δ_b and δ_r, we first use the microwave Ramsey spectroscopy to determine the qubit frequency ω_q whose measurement precision is on the order of $2\pi \times 5\,\mathrm{Hz}$; Then we use the Raman sideband Ramsey spectroscopy to determine the secular frequency ω_m of the ion motion whose measurement precision is on the order of $2\pi \times 100\,\mathrm{Hz}$; Finally, we set the two differential Raman laser frequencies at $\omega_\mathrm{q} + \omega_\mathrm{m} + \delta_b$

* These authors contribute equally to this work

† Corresponding author: lmduan@tsinghua.edu.cn

and $\omega_q - \omega_m + \delta_r$ respectively. Using the above method, the deviation of the actual value of $\delta_{b\,(r)}$ from the target value of $\delta_{b\,(r)}$ can be well bounded by the measurement precision of the secular frequency, i.e. the order of $2\pi \times 100\,\mathrm{Hz}$. This means the ratio parameter uncertainty for $R = 25$, 50, 75 and 100 is ± 1.3, ± 2.5, ± 3.8 and ± 5.0 respectively, i.e. roughly 5% relative error. Also the trap frequency fluctuation during the measurement is on the order of $2\pi \times 200\,\mathrm{Hz}$ (considering the $200\,\mathrm{s}^{-1}$ motional dephasing rate described below), this will induce about 10% ratio fluctuation in the experiment. This ratio calibration uncertainty and the ratio fluctuation during the measurement are the main error sources of the experimental data. In terms of the calibration for the sideband Rabi frequency Ω_{SB}, we just fix the laser beam intensity and scan the sideband Rabi oscillation for several cycles and fit out the Rabi frequency. The laser intensity fluctuation is below 1 %, hence the fluctuation of Rabi frequency is in the same order. This error has tiny effect to experiment data.

NOTE ON THE BREAKDOWN OF THE LINEAR APPROXIMATION OF THE RED SIDEBAND PULSE

The validity of our experiment is based on the assumption that we need to make sure that the cooling time duration τ_c is much smaller than the inverse of the red sideband Rabi rate Ω_c, therefore $\sin^2(\sqrt{n}\Omega_c\tau_c/2)$ can be linearized if the phonon number n is not too large. The consequence of going beyond is that when the experiment steps into the regime where the average phonon number of the state is too large, the terms in the high phonon number cannot be efficiently cooled down by using the red sideband pulse plus the optical pumping. Therefore, the steady state is hard to be reached in a practical numerical simulation time and may be very different from the prediction of the current model. However, with the average phonon number below 10, we have verified that the numerical simulations with or without the linear approximation have nearly the same consequence. Therefore, in our experimental regime, the red sideband pulse plus the spin reset can be well approximated by the dissipative channel $\hat{L} = \Omega_c\sqrt{\tau_c}\hat{a}/2$.

NUMERICAL AND EXPERIMENTAL INVESTIGATION OF THE DISSIPATIVE PHASE TRANSITION

Numerical investigation

To further prove the existence of a dissipative phase transition in our model and to understand the critical behavior, here we present numerical results for the finite-size scaling as the frequency ratio $R \equiv (\delta_b + \delta_r)/(\delta_b - \delta_r)$ approaches infinity. To obtain the steady state, we alternatingly simulate the unitary evolution under $\hat{H}_{\mathrm{QRM}}$ and the dissipative process governed by the Lindblad superoperator $\hat{L} = \Omega_c\sqrt{\tau_c}\hat{a}/2$ together with a spin reset as described in the main text. Note that these two processes are described in two different interaction pictures with $\Delta\hat{H}_0 \equiv \hat{H}_0' - \hat{H}_0 = \omega_a\hat{\sigma}_z/2 + \omega_f\hat{a}^\dagger\hat{a}$, thus a time-dependent relative phase needs to be included in the simulation when switching between the two interaction pictures. We repeat these two processes until the calculated average phonon number $\langle\hat{a}^\dagger\hat{a}\rangle$ converges.

Here we consider the same parameters as in the main text. That is, in each cycle the quantum Rabi model is applied for $\tau = 20\,\mu$s at varying sideband Rabi frequency Ω_{SB}; the sideband cooling pulse with $\Omega_c = 2\pi \times 20\,\mathrm{kHz}$ is applied for $\tau_c = 5\,\mu$s; additional $10\,\mu$s for optical pumping and idling time are included in the sideband cooling stage to give a total duration $\tau_d = 15\,\mu$s when computing the relative phase mentioned above. We fix $\delta_b - \delta_r = 2\pi \times 2\,\mathrm{kHz}$ and vary $\delta_b + \delta_r$ to set the ratio R from 50 to 3200. As shown in Fig. S1(a), we plot the average phonon number $\langle\hat{a}^\dagger\hat{a}\rangle$ versus the dimensionless coupling $g \equiv 2\Omega_{SB}/\sqrt{\delta_b^2 - \delta_r^2}$ from $g = 1.0$ to $g = 1.4$. For g below $g_c \approx 1.351$, the average phonon number in the steady state saturates to a finite value as we increase R; while for $g > g_c$, the steady state phonon number diverges in the limit $R \to \infty$ (note that for increasing R we need to use larger phonon number cutoff in the numerical simulation to suppress the truncation error). In Fig. S1(b) we plot the scaling behavior of the steady-state phonon number with respect to the ratio R at fixed g, and fit the numerical results to obtain the asymptotic form as R approaches infinity. As shown in the figure, for $g = 1.3$ in the weak coupling region the phonon number eventually saturates at $N_s = 1.54$, while for $g = 1.5$ in the strong coupling region a power-law scaling indicates an infinite steady-state phonon number as $R \to \infty$. This phenomenon of a diverging phonon number is similar to the case considered in Ref. [22] in the main text. In Fig. S1(c) we plot the saturation value N_s of the steady state phonon number in the limit $R \to \infty$ versus g in the $g < g_c$ region. We further fit the data near the critical point as $N_s = C(g_c - g)^{-\nu}$ as shown in the inset, from which we extract the critical point $g_c \simeq 1.351 \pm 0.002$ and a critical exponent $\nu \simeq 1.092 \pm 0.029$, the error bar is 1 S.D. from fitting. In Fig. S1(d), we plot the scaling behavior of the phonon number at the critical point $g_c = 1.351$, which fits a power-law behavior $\langle a^\dagger a\rangle \propto R^{0.531}$.

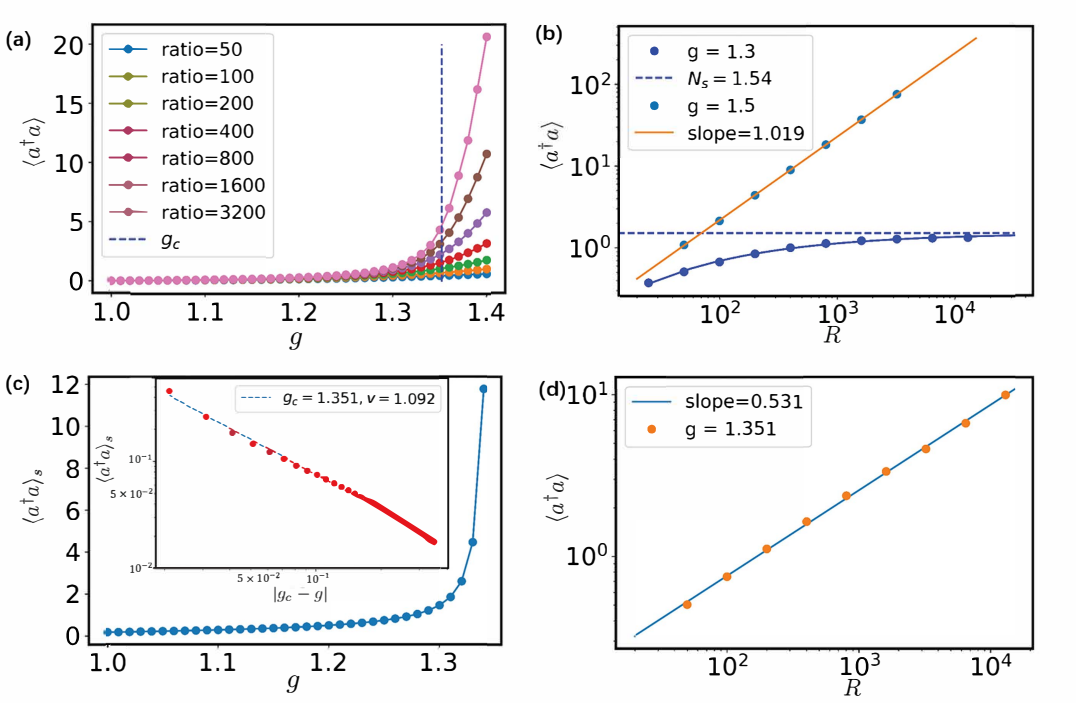

FIG. S1: **Numerical study of the dissipative phase transition.** **(a)** The steady state phonon number $\langle \hat{a}^\dagger \hat{a}\rangle$ versus the dimensionless coupling strength g at various ratio R ranging from 50 to 3200. **(b)** The steady state phonon number $\langle \hat{a}^\dagger \hat{a}\rangle$ versus the ratio parameter R at different coupling strengths ($g = 1.3$ and $g = 1.5$). In the weak coupling region ($g = 1.3$) the phonon number saturates as $R \to \infty$, while in in the strong coupling region ($g = 1.5$), the phonon number shows a power-law scaling with R and approaches infinity as $R \to \infty$. **(c)** The saturation value of the steady state phonon number $N_s \equiv \langle \hat{a}^\dagger \hat{a}\rangle_s$ in the limit $R \to \infty$ in the region $g < g_c$. By fitting $N_s = C(g_c - g)^{-\nu}$, we get the critical point $g_c \simeq 1.351$ and a critical exponent $\nu \simeq 1.092$, the error bar is 1 S.D. from fitting. **(d)** The scaling behavior near the numerically calculated critical point $g_c = 1.351$, which fits a slope of 0.531 in the log-log plot.

Experimental investigation

In order to see clear phonon number scaling with finite frequency ratio, we fix the coupling strength $g = 1.5$ and try to observe the average phonon number at different frequency ratio just like the result in Fig. S1(b). In order to have sufficiently large ratio R and experimentally feasible sideband Rabi rate Ω_{SB} (in our current condition, Ω_{SB} need to be smaller than $2\pi \times 20\,\mathrm{kHz}$ due to the laser intensity limitation) at $g = 1.5$, the $\delta_b - \delta_r$ need to be as small as possible. On the other hand, the precision of the parameter calibration is around $100Hz$. Thus we fix $\delta_b - \delta_r = 1\,\mathrm{kHz}$ as a tradeoff, resulting in the required Rabi rate $\Omega_{\mathrm{SB}} = 2\pi \times 7.5$, 10.6, 13.0, $15.0\,\mathrm{kHz}$ at $R = 100$, 200, 300, 400, respectively with around 10 % relative erorr in R. The result is shown in Fig. S2. We fit the experimental data with a linear line under the log-log scale shown as a blue line in the figure. The orange shaded region represents 0.95 confidence level (2 S.D.) band and the extracted slope of the blue line is 0.707 ± 0.148 (2 S.D.). The green line is calculated from the numerical simulation and the slope is around 0.843. We can see the experimentally extracted slope is smaller than the numerical result but is still reasonable considering relatively large error of the ratios. A more precise extraction of the critical exponent is limited by the current experimental noise. We need to further reduce the fluctuation of the experimental parameters such as the trap frequency, laser intensity etc. towards an observation of critical phenomena under this model.

NUMERICAL SIMULATION WITH SMALL RATIO INCREMENT

As the ratio increment is large enough, as shown in Fig. S1 the trend of the phonon number near the critical point shows a good phase transition behavior. However, in this dissipative phase transition model, we find that as the increment of ratio is small, the phonon number of the steady state has a small "back and forth" behavior, and shows

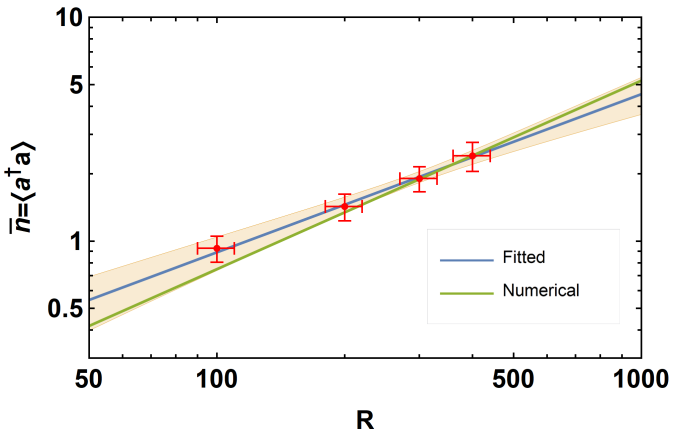

FIG. S2: **Average phonon number scaling.** The red dots are exprimental results with vertical error bars representing 1 S.D. and horizontal error bars estimated from calibration uncertainty. The blue line is a fitting result with the orange shaded region representing 0.95 confidence level (2 S.D.) band. The green line is from numerical simulation whose slope is around 0.843 representing the critical exponent.

a nonmonotonic behavior. In our simulation, we take two different series of the ratios, i.e. (300, 325, 350, 375, 400) and (500, 525, 550, 575, 600). We plot the steady state phonon number versus the dimensionless coupling coefficient g in two different regimes. The first regime is near the critical point, where gs are taken from 1.0 to 1.4. In this regime, as we increase the ratio with a small value (25), the steady state phonon number exhibits a small "back and forth" behavior as shown in Fig. S3 (a), (b). As the dimensionless coupling coefficient is far beyond the critical point (the second observation regime), the trend of the phonon number becomes monotonic, and no "back and forth" behavior is observed. Hence, although a small increment in the ratio may lead to a small "back and forth" behavior in the phonon number, the overall trend of our model still shows a clear phase transition.

NUMERICAL SIMULATION WITH NOISE

We further consider the decoherence effect in the numerical simulation. This can be simulated by invoking the Lindblad superoperator $L[\hat{O}]\hat{\rho} \equiv \hat{O}\hat{\rho}\hat{O}^\dagger - \hat{O}^\dagger\hat{O}\hat{\rho}/2 - \hat{\rho}\hat{O}^\dagger\hat{O}/2$. For motional heating and dephasing, the superoperator is $L[\sqrt{\gamma n_{\rm th}}\hat{a}^\dagger] + L[\sqrt{\gamma(n_{\rm th}+1)}\hat{a}]$ and $L[\sqrt{2\Gamma_m}\hat{a}^\dagger\hat{a}]$ respectively [1], where $\gamma n_{\rm th}$ is the heating rate and $\Gamma_{\rm m}$ is the dephasing rate. In our measurement, the motional dephasing rate $\Gamma_{\rm m}$ is around $200\,{\rm s}^{-1}$, the heating rate is below $50\,{\rm s}^{-1}$. It is not necessary to consider the effect of the spin dephasing because the duration ($\approx 20\,\mu$s) between the two spin resets is much smaller than the spin dephasing time of our system ($\approx 50\,$ms).

Besides, we consider another heating effect caused by the photon recoil from the optical pumping. Note that only when the ion is in the spin up state (i.e. the bright state) will it absorb photons. Hence the number of photons being absorbed by an ion is $N_b = N_p \times P_\uparrow$, where N_p indicates the average number of photons being absorbed by an ion during the optical pumping (in $^{171}{\rm Yb}^+$, $N_p = 3$), and $P_\uparrow$ is the population of the spin up state. The heating energy of the ion for each pumping step roughly equals to the recoil energy of the photons, which increases one of the three motional modes phonon number by $\frac{(N_b\hbar k)^2}{2m\times 3\omega_{\rm m}}$ with the photon wavevector k, the ion mass m and the motional mode frequency $\omega_{\rm m}$.

As shown in Fig. S4, the solid, dashed and dot-dashed lines are the simulation results of the variation of average phonon number versus the coupling strenghth g, without any noise effect, with only the decoherence effect and with both the decoherence and recoil effect, respectively. We can see the phonon number is slightly larger after considering the decoherence and recoil effect which is consistent with intuition.

[1] Q. A. Turchette, C. J. Myatt, B. E. King, C. A. Sackett, D. Kielpinski, W. M. Itano, C. Monroe, and D. J. Wineland, "Decoherence and decay of motional quantum states of a trapped atom coupled to engineered reservoirs," Phys. Rev. A **62**, 053807 (2000)

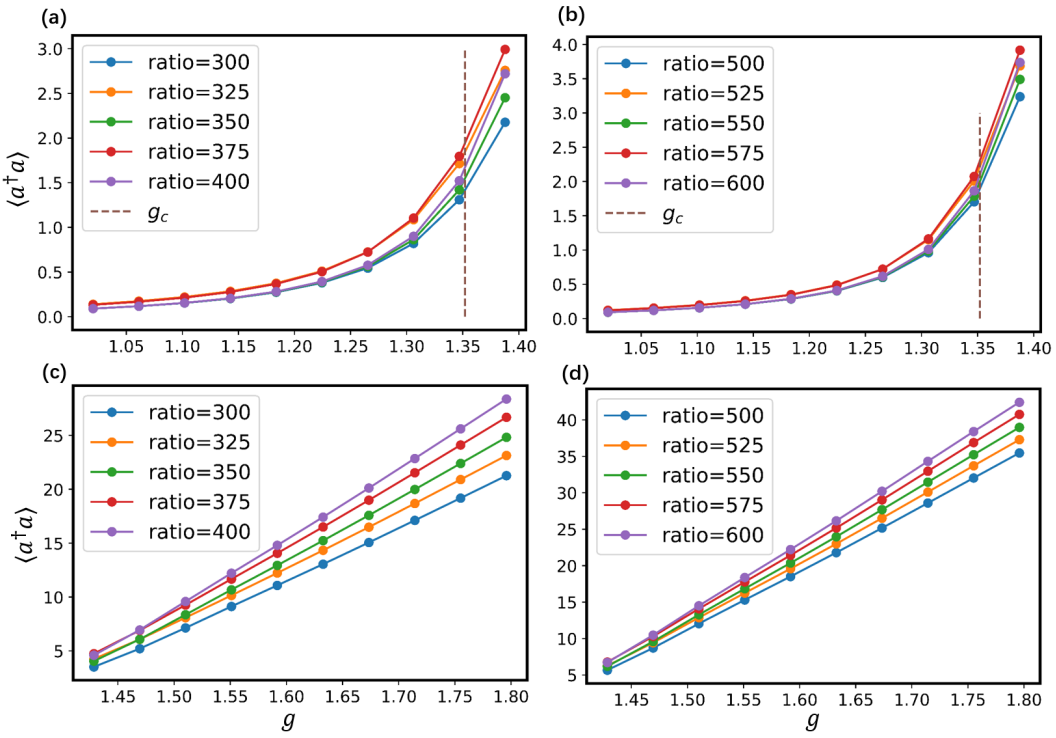

FIG. S3: **The trend with small ratio increment.** We plot the steady state phonon number with respect to different dimensionless coupling g with a small ratio increment 25 from 300 to 400 in **(a)**, **(c)** and 500 to 600 in **(b)**, **(d)**. **(a)** and **(b)** show the trend in the near-critical-point regime. **(c)** and **(d)** show the trend far beyond the critical point.

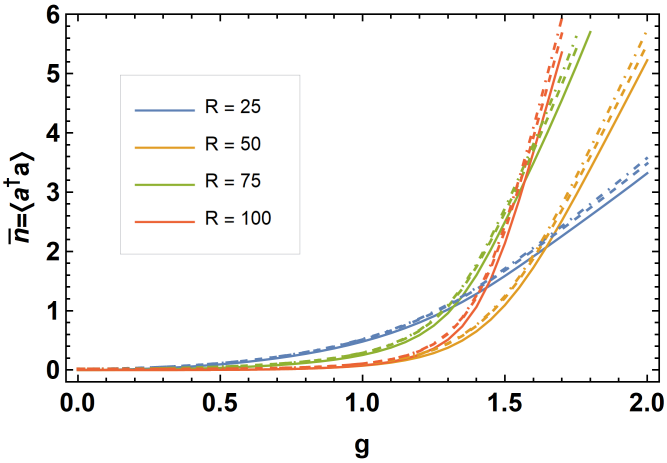

FIG. S4: **Numerical simulation with/without noise effect.** The solid, dashed and dot-dashed lines are the simulation results of the variation of average phonon number versus the coupling strength g, without any noise effect, with only the decoherence effect and with both the decoherence and recoil effect, respectively. It's obvious that the phonon number is slightly larger after considering the decoherence effect and recoil effect.

.